Published in final edited form as:
Mol Cell Neurosci. 2014 July ; 61: 226–240. doi:10.1016/j.mcn.2014.07.006.

Lysosome size, motility and stress response regulated by Fronto-Temporal Dementia modifier TMEM106B

Massimiliano Stagi[1,2,#], **Zoe A. Klein**[1,2], **Travis J. Gould**[3], **Joerg Bewersdorf**[3], and **Stephen M. Strittmatter**[1,2,*]

[1]Program in Cellular Neuroscience, Neurodegeneration & Repair, Yale University School of Medicine, New Haven, CT 06536, USA

[2]Department of Neurology, Yale University School of Medicine, New Haven, CT 06520, USA

[3]Department of Cell Biology, Yale University School of Medicine, New Haven, CT 06510, USA

Abstract

Fronto-Temporal Lobar Degeneration with TDP-43 (FTLD-TDP) is a fatal neurodegeneration. *TMEM106B* variants are linked to FTLD-TDP risk, and TMEM106B is lysosomal. Here, we focus on neuronal TMEM106B, and demonstrate co-localization and traffic with lysosomal LAMP-1. pH-sensitive reporters demonstrate that the TMEM106B C-terminus is lumenal. The TMEM106B N-terminus interacts with endosomal adaptors and other TMEM106 proteins. *TMEM106B* knockdown reduces neuronal lysosomal number and diameter by STED microscopy, and overexpression enlarges LAMP-positive structures. Reduction of TMEM106B increases axonally transported lysosomes, while TMEM106B elevation inhibits transport and yields large lysosomes in the soma. TMEM106B overexpression alters lysosomal stress signaling, causing a translocation of the mTOR-sensitive transcription factor, TFEB, to neuronal nuclei. TMEM106B loss-of-function delays TFEB translocation after Torin-1-induced stress. Enlarged TMEM106B-overexpressing lysosomes maintain organelle integrity longer after lysosomal photodamage than do control lysosomes, while small TMEM106B-knockdown lysosomes are more sensitive to illumination. Thus, neuronal TMEM106B plays a central role in regulating lysosomal size, motility and responsiveness to stress, highlighting the possible role of lysosomal biology in FTLD-TDP.

Introduction

FTLD is amongst the most prevalent neurodegenerative dementias after Alzheimer's. Symptomatology includes pronounced behavioral changes with altered motivation, personality and/or language function, with pathology in the frontal and temporal lobes

*Correspondence should be addressed to Stephen M. Strittmatter, CNNR Program, BCMM 436, Yale University School of Medicine, 295 Congress Avenue, New Haven, CT 06536 USA Tel +01-203-785-4878, FAX +-1-203-785-5030, stephen.strittmatter@yale.edu.
#Present address: Institute of Translational Medicine, Liverpool University, Liverpool, L693GL UK

(Mackenzie et al., 2010). The largest subset of FTLD exhibits neuronal TDP-43 aggregates. Common inherited causes of FTLD-TDP are repeat expansions in *C9ORF72*, and loss-of-function in the granulin (*GRN*) gene encoding progranulin (PGRN) protein. PGRN is internalized and concentrated in neuronal lysosomes after binding to Sortilin receptors (Hu et al., 2010). In one family, homozygous *GRN* mutation causes a lysosomal storage disorder (Smith et al., 2012). Thus, understanding of FTLD-TDP is intimately connected with the function of the neuronal lysosome.

A genome-wide association study of FTLD-TDP risk demonstrated linkage with polymorphisms near the *TMEM106B* locus (Van Deerlin et al., 2010). Risk association of *TMEM106B* variants was greatest for *GRN* mutation carriers, in which there was a decrease in the frequency of homozygous carriers of the rs1990622 minor allele (Van Deerlin et al., 2010; Finch et al., 2011). The most strongly associated SNP, rs1990622, is tightly linked to a missense T185S variant in TMEM106B (rs1042949), suggesting a protective effect of the p.185T form. This association has been replicated and extended to age of FTLD onset (Cruchaga et al., 2011), to clinical cohorts (van der Zee et al., 2011) and to cognitive change in ALS cohorts (Vass et al., 2011). There is evidence that this allele protects against hippocampal sclerosis pathology in those with Alzheimer's disease (Rutherford et al., 2012).

TMEM106B variation alters PGRN level in human serum (Cruchaga et al., 2011; Finch et al., 2011), but the cell biological basis of this effect is unclear. *TMEM106B* encodes a 274 aa transmembrane protein, and recent publications indicate that TMEM106B is predominantly localized at the endo-lysosomal membrane where it might interact indirectly with PGRN (Chen-Plotkin et al., 2012; Lang et al., 2012; Brady et al., 2013). However, TMEM106B's role in neurons and in lysosomal biology remains poorly defined. A report that appeared online while this manuscript was in preparation (Schwenk et al., 2014), describes TMEM106B interaction with MAP6 and a selective regulation on dendritic retrograde transport.

Recently, there have been advances in understanding lysosomal regulation. The transcription factor EB (TFEB) controls autophagy and lysosomal biogenesis by regulating expression of the Coordinated Lysosomal Expression and Regulation (CLEAR) gene network (Sardiello et al., 2009; Settembre et al., 2013). TFEB colocalizes with the mechanistic target of rapamycin complex 1 (mTORC1) on the lysosome. When nutrients are present, phosphorylation of TFEB by mTORC1 inhibits TFEB. Conversely, inhibition of mTORC1 or starvation or lysosomal disruption activates TFEB by promoting dephosphorylation and nuclear translocation (Settembre et al., 2012). TFEB acts to sense lysosome state at the lysosome and as an effector of lysosomal function when translocated to the nucleus. Lysosome-to-nucleus signaling allows organelle self-regulation (Settembre et al., 2012).

We sought to determine whether TMEM106B is present in the neuronal lysosome and whether it has a key role in determining organelle size, motility and stability. We report that depletion of neuronal TMEM106B reduces lysosome size and responsiveness to stress, but increases motility. These findings expand our understanding of lysosomal regulation and suggest these pathways contribute to FTLD-TDP pathophysiology.

Material and Methods

Plasmids and reagents

TMEM106B expression vectors under the chicken beta actin promoter were generated by amplifying the coding sequence of human TMEM106B-WT or TMEM106B-T185S full-length cDNAs (Origene, for both sequences) and cloning into the pCAGG vector via EcoRI sites. From pCAGG-human-TMEM106B-WT or T185S, a Cherry fluorescent protein tag was sub-cloned in frame immediately before the stop codon of TMEM via SmaI to obtain pCAGG-hTMEM106B-Cherry with WT or T185S. From pCAGG-human-TMEM106b, a pHlourin fluorescent protein tag was sub-cloned in frame to the carboxyl terminal of TMEM via SmaI to obtain pCAGG-hTMEM106B-pHlourin. Mouse TMEM106B was amplified from a full-length cDNA plasmid (Origene) and sub-cloned in frame into pCAGG-Cherry to obtain pCAGG-mTMEM106B-Cherry. Human TMEM106C was amplified from a full-length cDNA plasmid (Origene) and sub-cloned in frame into pCAGG-eGFP to obtain pCAGGS-hTMEM106C-eGFP. All constructs were sequence-verified.

PGRN and Sort1 clones have been described (Hu et al., 2010). Human PGRN was modified by insertion of a NheI restriction site after the signal peptide sequence using the site-directed mutagenesis kit (QuikChange Lightning; Agilent Technologies) according to the manufacturer's instructions, subcloned into pCAGG and eGFP inserted in frame by NheI to obtain pCAGG-hPGRN-eGFP.

The coding region for human TFEB-eGFP (a kind gift of Andrea Ballabio, Texas Children Hospital, USA (Sardiello et al., 2009)) was amplified by PCR and inserted in pDNA5.0 FRT TOPO (Life Technologies) to obtain pDNA5.0 FRT TFEB-eGFP. This vector was utilized to produce a Flp-In-293 stable cell line expressing TFEB-EGFP according the manufacturer's directions (Invitrogen). The human TFEB cassette was also subcloned in frame with pHlourin to obtain pCAGG-TFEB-GFP.

pCMV-Lamp1-RFP (Addgene 1817 (Sherer et al., 2003)) and rat LAMP1-eGFP were gifts from Roberto Zoncu, MIT, USA. The coding region for rat LAMP1-eGFP was amplified by PCR, and then subcloned into pCAGG via NheI to obtain pCAGG –LAMP1-eGFP.

The pLKO.1puro U6 shRNA mouseTMEM106b Ub TurboGFP plasmid, clone number TRCN0000174460, was validated for >85% knockdown efficiency (Sigma-Aldrich). Non-targeting pLKO.1puro U6 vector was obtained form the same source. Human siRNA pool targeting human TMEM106B (10 μM) was from Santa Cruz (sc-89400).

Torin-1 (Tocris) was used at final concentration of 250 nM (Thoreen et al., 2009; Roczniak-Ferguson et al., 2012; Settembre et al., 2012).

Neuronal culture

Dissociated mouse cortical neurons were prepared from C57BL/6 mice embryos (E18) as described (Hu et al., 2010; Um et al., 2012; Um et al., 2013). Tissue was dispersed mechanically and seeded in 8-well chamber culture dishes. The dishes were pretreated with poly-L-lysine (0.1mg/ml, Sigma, Germany) or alternatively on Matrigel (Becton-Dickinson

Biosciences). The cells were cultured in neurobasal A medium (Invitrogen) supplemented with 2% B-27 supplement, (Invitrogen) and 0.5% fetal calf serum (FCS, PAN Biotech). Cells were cultured for 20 days to obtain morphologically mature neurons and synapse formation. In the case of transfections, plasmids were purified using the EndoFree Maxi Kit (Qiagen). Transfection was performed using electroporation at the time of dissociation using an Nucleofector system (Amaxa), following the manufacturer's instructions and program O-005. The average transfection efficiency was from 30 to 70%, and the majority of transfected neurons showed plasmid expression from day 3-5 through day 30.

Spinning Disk Time Lapse Confocal Microscopy

HEK293 and COS7 cells were imaged 24-48 hours after transient transfections by the lipofectamine method (Invitrogen). Neurons were imaged after 20 days in culture. Images were collected at room temperature in modified Tyrode solution (pH 7.4) on a UltraView VoX Spinning Disk microscope with an auto focus system (Perkin-Elmer), a motorized XY stage, Piezo Z, 6 different laser lines (405 nm/50 mW, 445 nm/40 mW, 488 nm/50 mW, 514 nm/25 mW, 561 nm/50 mW, 640nm/50 mW diode laser) and Hamamatsu C9100-50 camera. All experiments were performed using 60× CFI Plan Apo VC, NA 1.4, oil. Images were captured at frame rates specified in the Figure Legends.

Two-Hybrid screening

Two independent yeast two-hybrid screens were carried out to identify interacting partners of TMEM106B. One screen utilized as bait the cytoplasmic fragment of TMEM106B (aa 1–96) and the other used the C-terminal lumen fragment of TMEM106B (aa 118–274). The prey library was derived from human adult brain using LexA fusion and 1.4×E8 interactions were screened (ULTImate Y2H, Hybrigenics Services).

Immunoprecipitation

Human embryonic kidney 293 (HEK293) cells were maintained in DMEM containing 10% FBS and 100 U/ml penicillin-streptomycin. To prepare cell lysates, transfected HEK293 cells were rinsed with ice-cold phosphate-buffered saline (PBS) and solubilized in lysis buffer containing Tris, pH 7.4, 1.0% Triton X-100, 0.1% SDS, 150 mM NaCl, 10% glycerol, complete protease inhibitor cocktail (Roche), phosphatase inhibitor (Roche). After centrifugation at 20,000 × *g* for 20 min at 4°C, the supernatant was collected for immunoprecipitation. Cherry-containing fusion proteins were immunoprecipitated using the anti-RFP antibody conjugated resin according to the manufacturer's instructions (RFP-Trap, Chromotek). The immunocomplexes were eluted from the resin and then resolved by SDS-PAGE and immunoblotted by the appropriate antibody.

Immunoblots

Precast 4-20% Tris-glycine or 10–20% Tris-tricine gels were used (Bio-Rad). After transfer, nitrocellulose membranes (Bio-Rad) were incubated in blocking buffer for 1 h at RT (Rockland, MB-070-010). Membranes were then washed three times in TBST, and incubated overnight in primary antibodies. The following primary antibodies were used: rabbit anti-RFP at 1:1000 (Rockland, 600-401-379), mouse anti-eGFP at 1:500 (Santa Cruz,

SC9996), rabbit anti-MITF at 1:500 (Millipore), rabbit anti-AP2M1 at 1:500 (a kind gift of Pietro De Camilli, Yale University, equivalent to Abcam, ab75995). All antibodies were diluted in blocking buffer, and membranes were incubated overnight at 4°C. Following primary antibody incubation, the membranes were washed three times with TBST, and secondary antibodies were applied for 1 h at RT (Odyssey goat anti-mouse or anti-rabbit IRDye 680 or 800). Membranes were then washed and proteins visualized using a Licor Odyssey Infrared imaging system.

Immunocytochemistry

DIV20 cortical neurons were fixed with 4% formaldehyde and 4% sucrose, permeabilized with 0.1 % Triton X-100 in PBS for 30 min, and washed with PBS. The samples were then blocked with 1% BlokhenII (Aves) for 30 min, and incubated overnight at 4°C with mouse Anti-Lamp1 primary antibody at 1:500 (Santa Cruz, SC19992). Then, either Alexa-Fluor-488 conjugated goat anti-mouse or Alexa-Fluor-568 conjugated goat anti-rabbit antibody (1:600 dilution) was used to detect the primary antibodies. Samples were mounted with mounting solution containing DAPI (Vector Laboratories). Sample ware mounted with Image-It FX signal enhancer (Invitrogen). Images were acquired on a LSM 710 META laser scanning confocal microscope (Zeiss) using 63× water objective, 40× air objective, 20× air objective, with channels scanned separately to avoid signal overlap and a pinhole set to optimal for each channel.

TMEM106B shRNA and mRNA measurement

Plasmid encoding U6-driven shRNA targeting mouse TMEM106B was introduced into neurons by Amaxa electroporation. Several shRNA species were tested and the optimal knockdown was achieved with Sigma-Aldrich, pLKO.1puro U6 RNAi, mouse TMEM106b, clone number TRCN0000174460. All data reported here are derived from use of this clone. For knockdown experiments, one set of neurons received the pLenti TMEM106b shRNA vector plus a Synapsin promotor-driven expression vector for soluble Cherry as a marker, and the other set received empty pLKO.1puro U6 RNAi vector and the Cherry marker vector. After 7-21 days in culture, neuronal cultures were analyzed for TMEM106B mRNA levels by quantitative real-time PCR analyses of mTMEM106b (TaqMan Tmem106b mouse Mm00510952_m1), as well as the control Actin mRNA transcripts. Measurements were conducted using an assay-on-demand gene-specific fluorescently labeled TaqMan MGB probe in an CFX96 Real Time System (BioRad).

Measurement of Lysosomal Traffic in Neuronal Processes

Kymographs were generated from time-lapse images of LAMP1-eGFP-expressing neurons by selecting 20-30 μm segments of axonal or dendritic processes immediately adjacent to the neuronal cell body. Projections were made along this segment in the time axis for 150 frames collected at 3 sec per frame. From these kymographs, moving and stationary LAMP1-eGFP-positive structures were identified and counted.

STED microscopy of Lysosome–labeled compartments

To visualize lysosomes with super resolution in neurons, we utilized anti-LAMP1 antibody with secondary antibody tagged with ATTO647N, a highly photostable dye that is useful for STED microscopy (Westphal et al., 2008). Neurons were imaged on a commercial STED microscope (TCS STED, Leica Microsystems) featuring a 640-nm pulsed excitation laser synchronized to the output of a Ti:Sapphire laser tuned to 770 nm for depletion of ATTO647N (Pellett et al., 2011). The line-scan rate was 1000 Hz, and the size of the detection pinhole was 0.5 airy units. The average background noise in a STED image was 0.4 counts/pixel, corresponding to a peak signal-to-background ratio of 65. The fluorescence profile, or the full width at half maximum (FWHM), of the STED-resolved spots approached the resolution limit (∼60 nm) of the microscope (Pellett et al., 2011). Large diffraction-limited spots that were seen with confocal imaging revealed themselves to be comprised of smaller spots when viewed in STED mode.

TFEB Nuclear Translocation

A clonal HEK293 cell line stably expressing TFEB-eGFP was obtained using the pDNA5.0 FRT TFEB-eGFP plasmid described above and culture conditions recommended by the Flp-In cell line supplier (Invitrogen). The pDNA5.0 FRT TFEB-eGFP expression vector allows incorporation of TFEB-eGFP upstream of a hygromycin resistance cassette in 293 Flp-In mammalian host cells. Single clones were isolated by hygromycin resistance and GFP expression confirmed.

qPCR Methods

HEK-293 cells were transfected with TMEM106b-cherry and TFEB-eGFP constructs for 48h in 24-well plates. Cells were washed 2× in ice cold PBS and immediately lysed for RNA extraction. RNA was purified using the Qiagen RNeasy Mini kit according to manufacturer's instructions. RNA was reverse-transcribed using the Bio-rad iScript cDNA Synthesis Kit according to the manufacturer's instructions. Real-time quantitative PCR was performed using the C1000 Thermal Cycler and quantified using the CFX96 Real-Time System (Bio-Rad). Samples were prepared using iTaq Universal Supermix (Bio-Rad). Taqman Primer-probe sets for the following genes were used: *ACTB* (Hs99999903_m1), *SGSH* (Hs00164924_m1), *TPP1* (Hs00166099_m1), *GLA* (Hs00609238_m1), *CSTB* (Hs00164368_m1). Samples were run in triplicate. Relative mRNA expression was calculated as gene of interest expression normalized to reference gene expression (*ACTB*). For each plate, template control (containing H_2O in place of template cDNA) was run to verify specificity of primer.

Acridine orange and lysosomal photo-oxidative damage

HEK293 cells or DIV20 neurons were preloaded for 10-20 minutes with 10 μg/ml acridine orange and then moved to the spinning disc imaging stage as described above. Cells were imaged in time lapse to capture signal in the rhodamine and fluorescein channels. Photodamage was induced by continuous illumination between images at 488 nm.

Statistical and image analysis

Datasets were compared using GraphPad Prism software. In general, data were analyzed by oneway ANOVA with post-hoc pairwise comparisons with Tukey correction for multiple tests. The 4D and 3D movies were generated using a combination of ImageJ (Fiji), Volocity (Perkin Elmer), Matlab (Mathworks) and Quick Time (Apple).

Results

TMEM106B protein is localized to neuronal lysosomes

To assess the subcellular localization of TMEM106B, we expressed fluorescently tagged protein in COS-7 cells. In single images of live cells, there was strong co-localization with the lysosomal markers, LAMP-1 and PGRN (not shown). Moreover, these markers moved in concert during time-lapse imaging (Movie 1). These observations match previous reports using fixed samples inimmortalized cell lines (Chen-Plotkin et al., 2012; Lang et al., 2012; Brady et al., 2013).

To assess the relevance to FTLD, we extended this analysis to live imaging of mouse cortical neurons at 20DIV. In primary neuronal cultures, there is striking colocalization between Lamp1 and TMEM106B (Suppl. Fig. S1). In addition, time-lapse imaging shows that these two markers are co-transported bidirectionally in neuronal processes (Movie 2). Thus, we conclude that TMEM106B protein localizes to neuronal lysosomes.

Amino terminus of TMEM106B is cytoplasmic

The TMEM106B primary sequence has a single hydrophobic segment and no signal sequence. To assess TMEM106B membrane topology, we made use of a pH sensitive GFP variant. We examined COS7 cells expressing TMEM106b with C-terminal Cherry tag plus a TMEM106b C-terminal pHluorin (Fig. 1A). The TMEM106b C-terminal pHluorin fluoresces only in those compartments of the sorting pathway with a pH near neutrality, but not within the acidic lysosomal lumen. The TMEM106b C-terminal Cherry tag is pH-insensitive and is evident in lysosomal-like structures under routine culture conditions (Fig. 1B). In contrast, there is little or no fluorescence from the pHluorin tag under these conditions (Fig. 1B, top). To raise the lysosomal lumen to neutral pH, we blocked proton uptake with bafilomycin A1 (500 nM) and alkalinized the medium with sodium bicarbonate. The alkalinization reduces lysosomal movement, and green fluorescence from the TMEM106b C-terminal pHlourin is unquenched and observed to colocalize with TMEM106b C-terminal Cherry (Fig. 1B, C, Movie 3). Indeed, the pHlourin channel fluorescence increased 3 fold with treatment to neutralize the lysosomal lumen, without any change in the Cherry fluorescence (Fig. 1D). Thus, we conclude that lysosomal TMEM106B is a transmembrane protein with a cytosolic N-terminus and a luminal C-terminus. Our conclusion from live cell imaging is consistent with that obtained from cell fractionation studies (Lang et al., 2012).

Cytoplasmic domain of TMEM106B interacts with endocytic proteins as a heteromultimer

To reveal potential functions of different TMEM106B domains based on interaction partners, we conducted separate yeast two-hybrid screens with the cytoplasmic or luminal

domains of TMEM106B.In one screen, we utilized as bait the cytoplasmic fragment of TMEM106B (aa 1–96), and in the other we employed the C-terminal (luminal) fragment of TMEM106B (aa 118–274) (Fig 2A). For the cytosolic N-terminal fragment, we detected interactions with the endocytic adaptor proteins, AP2M1 (the μ1 subunit of AP2) and CLTC (clathrin heavy chain), whereas no interactions were identified for the luminal C-terminal fragment. This is consistent with the C-terminal domain being present in the lysosomal lumen at acidic pH and not having interaction partners at cytoplasmic pH that might mediate nuclear complex formation in the two-hybrid screen. To validate the yeast two-hybrid result, we examined immunoprecipitates of tagged TMEM106B and detected endogenous AP2M1 and CLTC proteins (Fig. 2B and not shown). The proteins VPS11 and VPS13D also interacted with TMEM106B cytoplasmic domain in yeast two-hybrid assays. These proteins have a role in late endosomes to early lysosome traffic (Bankaitis et al., 1986; Banta et al., 1988; Rieder and Emr, 1997; Sato et al., 2000; Rampoldi et al., 2001; Park and Neiman, 2012). Unfortunately, available antibodies did not detect endogenous VPS11 or VPS13D, so we could not assess these interactions with TMEM106B by immunoprecipitation. Nonetheless, interactions with AP2M1 and CLTC are consistent with TMEM106B playing a role in recognition and/or delivery of endocytic cargos to the lysosome.

The N-terminal yeast two-hybrid screen also revealed interaction with a second TMEM106 family member, TMEM106C (Fig. 2A). The TMEM106C protein shares high sequence similarity (47% aa identity and 63% aa similarity) and domain structure with TMEM106B, but has no known function. This suggests that the TMEM106 family may form heteromeric and homomeric complexes at the lysosomal surface. To assess the composition of TMEM106 complexes, we examined co-immunoprecipitation of C-terminal Cherry tagged TMEM106B with either C-terminal eGFP tagged TMEM106B or TMEM106C. Control experiments with cells expressing the XFP domains alone show that anti-Cherry immunoprecipitates do not contain co-expressed eGFP (Fig. 2C). However, Cherry-TMEM106B immunoprecipitates either TMEM106B or TMEM106C with very high efficiency (Fig. 2D, E). The specificity of this interaction was further verified by the lack of interaction with the cytosolic MITF protein (Fig. 2E). Expression of TMEM106C in COS-7 cells reveals enrichment in the lysosomal compartment, colocalizing with LAMP1, and similar to TMEM106B (Fig. 2F). When TMEM106C is co-expressed with TMEM106B, both proteins are observed in the same puncta of COS-7 (Fig 2G) and neurons (Fig. 2H). The TMEM106 family appears to exist as both homo- and hetero-multimers at the lysosomal membrane.

TMEM106B expression determines lysosomal size in primary neurons

As a first step to understand how TMEM106B influences lysosomal physiology, we overexpressed the protein in HEK293 cells. We observed an increase in lysosomal area occupied by LysoTracker dye or anti-LAMP1 immunohistology (not shown). This confirms previous observations from overexpression in other immortalized cell lines (Chen-Plotkin et al., 2012; Brady et al., 2013).

We considered whether cerebral cortex neurons also exhibit regulation of lysosomal size by TMEM106B overexpression. For DIV20 primary cortical neurons, increasing TMEM106B

level yields a more than two-fold ($P \leq 0.01$) enlargement of the lysosomal compartment marked by co-expressed LAMP1-eGFP (Fig. 3A), or by immunohistology with anti-LAMP1 antibody (Fig. 3B). No change in lysosomal number is detected with TMEM106B overexpression (Fig. 3C). More critically, we suppressed endogenous neuronal TMEM106B expression using a U6-driven shRNA targeting *TMEM106B*. The mRNA levels for *TMEM106B* are reduced by expression of this shRNA to 25% of those in cultures with control vector, while actin levels are unchanged (Fig. 3D). As described previously (Schwenk et al., 2014), TMEM106B suppression increases dendritic branching (Suppl. Fig. S3). Neither TMEM106B suppression or overexpression altered neuronal cell viability or qualitative appearance of neuronal cultures at DIV20 (not shown). However, suppression of TMEM106 shows a non-significant trend of decreasing lysosomal size (Fig. 3B), and a strongly significant effect of decreasing lysosomal number (Fig. 3C; $P \leq 0.01$). These data show that endogenous neuronal TMEM106B is a key stabilizer of the lysosome, either by enhancing lysosomal biogenesis or survival.

A limitation to detecting a statistically significant reduction in the size of neuronal lysosomes by standard confocal microscopy after decreasing TMEM106B expression is the small size of these organelles in neurons. To determine whether TMEM106B has a bidirectional effect on lysosomal size, we utilized super resolution STED microscopy to image anti-LAMP1 immunohistology (Fig. 3E, F). Within the neurites of cortical neurons, knockdown of TMEM106B significantly reduced lysosome size to less than half of control lysosome area (Fig. 3G, $P \leq 0.01$). Thus, within neurons, endogenous TMEM106B plays a role in determining both lysosome number and size.

Lysosomal motility is regulated by TMEM106B expression

It is clear that TMEM106B plays a central role in determining lysosomal size in neurons. Another key aspect of lysosomal neurobiology is their transport within dendrites and axons. In DIV20 cortical cultures, single LAMP1-eGFP positive lysosomes are readily imaged in live cells within both soma and dendrites (Fig. 4A). As expected, LAMP1-eGFP positive puncta with co-expressed TMEM106b-cherry are larger. By time lapse imaging, saltatory lysosomal transport within neuronal process is readily apparent with time lapse imaging of LAMP1-eGFP (Movie 2).

We analyzed LAMP1-eGFP traffic in cultures with increased or decreased TMEM106B expression. Overexpression of TMEM106B strongly suppresses transport, such that fewer than 10% of LAMP1 positive organelles are mobile (Fig. 4B, C, Movie 4; $P \leq 0.001$). In contrast, TMEM106B suppression with shRNA increases the fraction of moving lysosomes from 50% to 80% (Fig. 4B, C, Movie 4; $P \leq 0.01$).

To assess whether there is an effect of TMEM106B on the direction of LAMP1-eGFP transport, we monitored transport in proximal dendrites in low density, less mature cultures at DIV8 (Fig. 4D). Similar overall effects of TMEM106B level on the fraction of transported LAMP1-positive structures is observed in these cultures (Fig. 4E). There is a non-significant trend for overexpression of TMEM106B to favor retrograde transport (Fig. 4F, G), but the major effect is for bidirectional transport. In addition, we noticed a tendency for lysosomes to accumulate close to the cell body in control and TMEM106B-

overexpressing neurons, whereas the more mobile lysosomes in TMEM106B shRNA neurons were distributed more distally throughout the neurites (Fig. 4A, B). Thus, neuronal TMEM106B titrates the size, motility and position of neuronal lysosomes.

The TFEB reporter of lysosomal stress correlates with TMEM106b expression

The TFEB transcription factor provides a reporter of lysosomal stress. When cells are healthy, TFEB is localized outside of the nucleus. Under conditions that cause lysosomal stress, the protein moves from cytosolic and lysosomal compartments into the nucleus to activate lysosomal genes (Sardiello et al., 2009). We considered whether TMEM106B levels might regulate the extent of TFEB translocation to the nuclear compartment. As a first step, we compared HEK293 cells stably expressing TFEB–GFP with or without expression of TMEM106B-Cherry. The expression of TMEM106B-Cherry, but not other lysosomal proteins such as LAMP1–RFP, caused a strong increase in nuclear TFEB, from less than 10% to greater than 80% of cells (Fig 5A,B; $P \leq 0.001$). Knockdown of TMEM106B with RNAi directed against human TMEM106B did not alter TFEB–GFP nuclear localization. The TMEM106B-Cherry overexpression effect on nuclear TFEB–GFP is independent of aa residue 185 variation from T to S (Fig. 5B).

A nuclear shift of TFEB is predicted to increase the expression of CLEAR network genes, so TMEM106B overexpression should exert the same effect as TFEB overexpression. In HEK293, we monitored gene expression by qPCR for 4 CLEAR network genes (Fig. 6). Overexpression of TMEM106B was as effective as that of TFEB to increase the levels of mRNA for SGSH, TPP1, CSTB and GLA. Thus, the ability of TMEM106B to drive TFEB nuclear localization appears functionally relevant for lysosomal protein regulation.

The regulation of TFEB and related lysosomal control proteins has not previously been described in primary neurons. Expression of fluorescently tagged TFEB under standard unstressed culture conditions yields a non-nuclear distribution, present in the cell soma (Fig 7A). The absence of nuclear protein is most obvious in Z stacks of the cell body showing a void in the nuclear location (Fig. 7B,C). The TFEB-GFP protein is also present in axons and dendrites, including dendritic spines (Fig. 7D).

Given the baseline non-nuclear TFEB-GFP localization, we compared neurons expressing TMEM106B-Cherry to those with TMEM106B shRNA or control vector (Fig. 7E, F). The percentage of control or TMEM106B knockdown neurons with nuclear TFEB was less than 5%, but more than 30% of TMEM106B overexpression neurons exhibited nuclear TFEB-GFP (Fig. 7F; $P \leq 0.001$). Thus, high levels of neuronal TMEM106B signal lysosomal stress, as well as immobilize lysosomal transport. The TMEM106B overexpression-induced nuclear translocation of TFEB increases the expression of CLEAR lysosomal genes, which may contribute to greater lysosomal size.

Since TMEM106B overexpression induces TFEB nuclear translocation, we hypothesized that reduced TMEM106B might limit the TFEB lysosomal stress response. By time-lapse imaging, we monitored the ability of bath application of Torin-1, an inhibitor of mTOR signaling (Thoreen et al., 2009; Roczniak-Ferguson et al., 2012; Settembre et al., 2012), to induce TFEB-GFP redistribution to the nucleus as a function of TMEM106B level (Fig. 8).

In control Cherry-expressing cells, nuclear TFEB-GFP increases gradually from 10-60 minutes. In TMEM106B-Cherry-expressing cells, nuclear TFEB-GFP levels are high at baseline, and increase only slightly. The timing of Torin-1-induced nuclear TFEB-GFP translocation is slower in TMEM106B shRNA knockdown neurons, with little if any change during the first 40 minutes (Fig. 8). Thus, TMEM106B participates in the sensitivity of neuronal lysosomes to stress.

TMEM106B modulates lysosomal stability to photo-oxidative damage

We sought to determine whether TMEM106B-mediated changes in lysosomal size, transport and TFEB regulation would alter the ability of the neuronal lysosome to respond to damage from reactive oxygen species. For these studies, we utilized the acridine orange (AO) dye, which specifically accumulates in the acidic lysosome compartment. When loaded cells are illuminated with blue light, lysosomal AO produces reactive oxygen species that damage the lysosomal membrane and cause dye leakage into the neutral pH environment of the cytoplasm where its fluorescence emission is reduced and shifted from red to green (Zdolsek et al., 1990; Kirkegaard et al., 2010). Abrupt disruption of individual lysosomal membranes as discrete “explosions” from lysosomal red to cytoplasmic green is readily apparent in time lapse imaging under blue illumination (Movie 5). HEK293 cells overexpressing TMEM106B without a fluorescent protein fusion show enlarged AO-positive lysosomal punctae compared to vector control cells (Fig. 9A). Time lapse imaging demonstrates that AO lysosomal fluorescence is lost over 7 minutes in control cells, but is preserved longer, for at least 10 minutes, in TMEM106B-overexpressing cells (Fig. 9A-C, Movie 5; $P \leq 0.001$). Thus, high levels of TMEM106B protect AO-loaded lysosomes from oxidative damage in immortalized cell lines.

We sought to determine whether neuronal lysosomes also exhibit TMEM106B regulation of sensitivity to reactive oxygen species. Loading of neurons with AO yielded high sensitivity of lysosomes to blue light, with loss of fluorescence with 1 to 2 minutes, substantially faster than HEK293 cells under the same conditions (Fig. 9D-E). We compared the rate of AO signal loss in neurons with endogenous TMEM106B to those overexpressing TMEM106B and those with TMEM106B knockdown. The rate of loss was significantly accelerated in neurons with reduced TMEM106B (Fig. 9D-E; $P \leq 0.01$), and there was a non-significant trend of delayed loss in neurons with greater TMEM106B. Thus, neuronal lysosomes require TMEM106B for robust protection against photo-oxidative damage.

Discusssion

This study provides multiple lines of evidence that the FTLD-TDP risk-related protein, TMEM106B, plays a crucial role in regulating neuronal lysosomes. In neurons, the TMEM106B protein localizes to lysosomes, where its cytoplasmic domain interacts with endo-lysosomal adaptors and forms multimers. This localization leads to changes in lysosomal size with a direct correlation of neuronal TMEM106B level with lysosome size and number. Active transport of lysosomes in neuronal processes is inversely correlated with TMEM106B levels. TFEB is a marker of lysosomal stress that directs the synthesis of lysosomal constituents when translocated to the nucleus. TMEM106B overexpression constitutively enhances TFEB translocation, while TMEM06B reduction impairs TFEB

activation. Photo-oxidative damage to the lysosomal membrane of neurons is delayed by elevation of TMEM06B expression, and is accelerated by TMEM106B suppression. These results define TMEM106B as a central regulator of the neuronal lysosome and they suggest the possibility of a key role for lysosomes in FTLD-TDP pathophysiology.

The localization of TMEM106B to the endo-lysosomal pathway is highly specific. Previous studies have reported this localization in several cell lines and neurons (Chen-Plotkin et al., 2012; Lang et al., 2012; Brady et al., 2013). Our time-lapse analysis of LAMP1 and TMEM106B co-traffic in neuronal organelles provides a dramatic confirmation of this point. Consistent with a role in endocytic traffic to the lysosome, we describe interactions with the μ1 subunit of AP2 endocytic adaptor, and with the heavy chain of the endocytic coat protein clathrin. VPS11 and VPS13D are TMEM106B interactors known to participate in endocytic vesicle maturation and in delivery to lysosomes (Bankaitis et al., 1986; Banta et al., 1988; Rieder and Emr, 1997; Sato et al., 2000; Rampoldi et al., 2001; Park and Neiman, 2012). These molecular interactions of TMEM106B may participate in the delayed degradation of endocytic cargoes in non-neuronal cells reported with TMEM106B overexpression (Brady et al., 2013).

Analysis of TMEM106B molecular interaction also indicates that the cytoplasmic N-terminus can associate with other TMEM106 family members. Both TMEM106B homo-oligomers and TMEM106B/C hetero-oligomers are observed by co-immunoprecipitation and immunohistology. The role of oligomerization in TMEM106 functional effects on lysosomal pathways and its dynamic regulation will merit future study. The interaction of TMEM106B with TMEM106C suggests that there may be at least partial redundancy in the TMEM106 family.

The level of TMEM106B strongly affects the nuclear translocation of the master lysosomal regulatory factor, TFEB. Higher levels of TMEM106B constitutively activate TFEB as measured by nuclear translocation of this transcription factor that activates the CLEAR network. Suppression of endogenous TMEM106B expression in neurons limits the response of TFEB to mTOR inhibition by Torin-1. Elevated TMEM106B level phenocopies mTOR inhibition with respect to TFEB localization and lysosomal size. TFEB plays a key role in linking lysosomal auto-regulation by starvation and mTORC-1 to autophagy (Settembre et al., 2011; Roczniak-Ferguson et al., 2012; Settembre et al., 2012). Thus, higher TMEM106B expression levels in neurons are predicted to enhance baseline autophagy. The interaction of TMEM106B levels with TFEB phosphorylation by mTOR and with Rag GTPase signaling are sites for future mechanistic investigation.

TFEB is the best-studied member of a family of related transcription factors including MITF and TFE3 (microphthalmia transcription factor and transcription factor E3). Similar to TFEB, these family members are localized to lysosomes and translocate to the nucleus with stress (Roczniak-Ferguson et al., 2012). In neurons, one or more of these proteins may be regulated by endogenous TMEM106B levels. The expression level, phosphorylation and subcellular localization of this protein family have not yet been studied in FTLD-TDP or in other neurodegenerative dementias.

An obvious effect of TMEM106B expression level is a change in lysosomal size and number. Suppression of endogenous TMEM106B in neurons yields lysosomes of smaller size and number. Super resolution microscopic techniques were required to document this effect on lysosomal size. The connection of TMEM106B level to TFEB nuclear translocation may explain changes in lysosomal size and number through activation of the constellation of structural lysosomal genes in the CLEAR network.

Neuronal TMEM106B levels also modulate the transport of lysosomes in neuronal processes. A greater proportion of the smaller TMEM106B-deficient lysosomes are transported than control LAMP1 organelles, while enlarged TMEM106B-enriched lysosomes accumulate in the cell soma and do not migrate. These changes seem quite likely to be secondary to impingement of TMEM106B on TFEB activation, the CLEAR network and lysosomal size. Alternatively, TMEM106B might alter specific transport mechanisms for lysosomes in addition to general TFEB autoregulatory control. For example, TMEM106B interaction with MAP6 was implicated in selective alterations of dendritic retrograde transport of lysosomes by one recent study (Schwenk et al., 2014). Here, we did not observe a differential effect on retrograde versus anterograde transport in dendrites after alteration of TMEM106B levels. This may very well be due to the use of different markers, LAMP1 here versus Rab7 in the previous study, or to different neuronal populations, cortical cultures here versus hippocampal cultures in the previous study.

To assess the net effect of TMEM106B regulation of lysosomal function, we investigated organelle integrity after photo-oxidative damage triggered by blue light illumination of the lysosomal dye, acridine orange (Zdolsek et al., 1990; Kirkegaard et al., 2010). Elevated TMEM106B level protects lysosomes from membrane disruption and leakage of dye, while reduced levels render the lysosome more sensitive to photo-oxidative damage. As for lysosomal size, these findings suggest that the direct correlation between TMEM106B level and TFEB nuclear translocation leads to more robust lysosomes. Multiple members of the CLEAR network rather than TMEM106B directly are likely to be responsible for increased lysosomal resistance to photo-oxidative damage. Regardless of whether this effect is direct or indirect through TFEB/CLEAR signaling, reduced TMEM106B renders lysosomes more fragile.

The human linkage of FTLD-TDP risk to TMEM106B allele suggests that T185S variation plays a role. While this genetic variation alters PGRN levels in serum (Cruchaga et al., 2011; Finch et al., 2011), the effect may be direct or indirect. Tissue culture studies reveal either small or no effect of TMEM106B variants on PGRN levels (Lang et al., 2012; Brady et al., 2013). A recent study described reduced protein stability for the T185S variant (Nicholson et al., 2013), suggesting that the protective T allele may elevate TMEM106B. The studies presented here would suggest that elevated TMEM106B would generate greater TFEB activation and greater lysosomal and autophagy function, which may be protective for TDP-43 pathology. In our cell culture studies, any effect of the human variant was subtle and further in vivo experimental analysis is required to fully understand the human disease linkage.

It is clear from this analysis that TMEM106B plays a key role in the regulation of neuronal lysosomes. This provides further rationale for considering lysosomal dysfunction central in FTLD-TDP. Additional observations supporting a specific role for lysosomal dysfunction in FTLD-TDP derive from studies of the common causative *GRN* gene. The PGRN protein accumulates in neuronal lysosomes (Hu et al., 2010), and humans homozygous for *GRN* loss of function suffer from neuronal ceroid lipofuscinosis (Smith et al., 2012). Furthermore, there exist endogenous GRN-cathepsin fusion proteins in plant species (Avrova et al., 1999; Yamada et al., 2001; Chen et al., 2006; Gu et al., 2012). The less common FTLD causative genes, *CHMB2B* and *VCP*, also participate in the endo-lysosomal pathway (Ju et al., 2009; Urwin et al., 2010). In addition, the lysosomal protease asparaginyl endopeptidase-1 (AEP-1, legumain) is responsible for endogenous cleavage of TDP-43 (Herskowitz et al., 2012). TDP-43 levels and aggregates are known to be titrated by autophagy, as well as proteosomal activity, and activation of autophagy ameliorates mouse model TDP-43 transgenic phenotypes (Wang et al., 2012).

Conclusions

These studies show that TMEM106B levels determine the setpoint for lysosomal auto-regulation by TFEB pathways in neurons. Levels of TMEM106B regulate lysosomal size, transport within the neuron and the resilience of the lysosome to photo-oxidative stress. The influence of TMEM106B genetic variation on the risk of FTLD-TDP highlights the potential role of lysosomal dysfunction in this neurodegenerative dementia.

Supplementary Material

Refer to Web version on PubMed Central for supplementary material.

Acknowledgments

We thank Andrea Ballabio, Roberto Zoncu and Pietro De Camilli for reagents, and Thihan Padukkavidana for assistance with acridine orange. This work was supported by grants to S.M.S. from the Association for Frontotemporal Degeneration, the National Institutes of Health and the Falk Medical Research Trust.

References

Avrova AO, Stewart HE, De Jong WD, Heilbronn J, Lyon GD, Birch PR. A cysteine protease gene is expressed early in resistant potato interactions with Phytophthora infestans. Molecular plant-microbe interactions: MPMI. 1999; 12:1114–1119. [PubMed: 10624019]

Bankaitis VA, Johnson LM, Emr SD. Isolation of yeast mutants defective in protein targeting to the vacuole. Proc Natl Acad Sci U S A. 1986; 83:9075–9079. [PubMed: 3538017]

Banta LM, Robinson JS, Klionsky DJ, Emr SD. Organelle assembly in yeast: characterization of yeast mutants defective in vacuolar biogenesis and protein sorting. The Journal of cell biology. 1988; 107:1369–1383. [PubMed: 3049619]

Brady OA, Zheng Y, Murphy K, Huang M, Hu F. The frontotemporal lobar degeneration risk factor, TMEM106B, regulates lysosomal morphology and function. Hum Mol Genet. 2013; 22:685–695. [PubMed: 23136129]

Chen HJ, Huang DJ, Hou WC, Liu JS, Lin YH. Molecular cloning and characterization of a granulin-containing cysteine protease SPCP3 from sweet potato (Ipomoea batatas) senescent leaves. Journal of plant physiology. 2006; 163:863–876. [PubMed: 16777534]

Chen-Plotkin AS, Unger TL, Gallagher MD, Bill E, Kwong LK, Volpicelli-Daley L, Busch JI, Akle S, Grossman M, Van Deerlin V, Trojanowski JQ, Lee VM. TMEM106B, the risk gene for

frontotemporal dementia, is regulated by the microRNA-132/212 cluster and affects progranulin pathways. J Neurosci. 2012; 32:11213–11227. [PubMed: 22895706]

Cruchaga C, Graff C, Chiang HH, Wang J, Hinrichs AL, Spiegel N, Bertelsen S, Mayo K, Norton JB, Morris JC, Goate A. Association of TMEM106B gene polymorphism with age at onset in granulin mutation carriers and plasma granulin protein levels. Arch Neurol. 2011; 68:581–586. [PubMed: 21220649]

Finch N, et al. TMEM106B regulates progranulin levels and the penetrance of FTLD in GRN mutation carriers. Neurology. 2011; 76:467–474. [PubMed: 21178100]

Gu C, Shabab M, Strasser R, Wolters PJ, Shindo T, Niemer M, Kaschani F, Mach L, van der Hoorn RA. Post-translational regulation and trafficking of the granulin-containing protease RD21 of Arabidopsis thaliana. PLoS One. 2012; 7:e32422. [PubMed: 22396764]

Herskowitz JH, Gozal YM, Duong DM, Dammer EB, Gearing M, Ye K, Lah JJ, Peng J, Levey AI, Seyfried NT. Asparaginyl endopeptidase cleaves TDP-43 in brain. Proteomics. 2012; 12:2455–2463. [PubMed: 22718532]

Hu F, Padukkavidana T, Vaegter CB, Brady OA, Zheng Y, Mackenzie IR, Feldman HH, Nykjaer A, Strittmatter SM. Sortilin-mediated endocytosis determines levels of the frontotemporal dementia protein, progranulin. Neuron. 2010; 68:654–667. [PubMed: 21092856]

Ju JS, Fuentealba RA, Miller SE, Jackson E, Piwnica-Worms D, Baloh RH, Weihl CC. Valosin-containing protein (VCP) is required for autophagy and is disrupted in VCP disease. The Journal of cell biology. 2009; 187:875–888. [PubMed: 20008565]

Kirkegaard T, Roth AG, Petersen NH, Mahalka AK, Olsen OD, Moilanen I, Zylicz A, Knudsen J, Sandhoff K, Arenz C, Kinnunen PK, Nylandsted J, Jaattela M. Hsp70 stabilizes lysosomes and reverts Niemann-Pick disease-associated lysosomal pathology. Nature. 2010; 463:549–553. [PubMed: 20111001]

Lang CM, Fellerer K, Schwenk BM, Kuhn PH, Kremmer E, Edbauer D, Capell A, Haass C. Membrane orientation and subcellular localization of transmembrane protein 106B (TMEM106B), a major risk factor for frontotemporal lobar degeneration. J Biol Chem. 2012; 287:19355–19365. [PubMed: 22511793]

Mackenzie IR, et al. Nomenclature and nosology for neuropathologic subtypes of frontotemporal lobar degeneration: an update. Acta Neuropathol. 2010; 119:1–4. [PubMed: 19924424]

Nicholson AM, Finch NA, Wojtas A, Baker MC, Perkerson RB 3rd, Castanedes-Casey M, Rousseau L, Benussi L, Binetti G, Ghidoni R, Hsiung GY, Mackenzie IR, Finger E, Boeve BF, Ertekin-Taner N, Graff-Radford NR, Dickson DW, Rademakers R. TMEM106B p.T185S regulates TMEM106B protein levels: implications for frontotemporal dementia. Journal of neurochemistry. 2013; 126:781–791. [PubMed: 23742080]

Park JS, Neiman AM. VPS13 regulates membrane morphogenesis during sporulation in Saccharomyces cerevisiae. J Cell Sci. 2012; 125:3004–3011. [PubMed: 22442115]

Pellett PA, Sun X, Gould TJ, Rothman JE, Xu MQ, Correa IR Jr, Bewersdorf J. Two-color STED microscopy in living cells. Biomed Opt Express. 2011; 2:2364–2371. [PubMed: 21833373]

Rampoldi L, Dobson-Stone C, Rubio JP, Danek A, Chalmers RM, Wood NW, Verellen C, Ferrer X, Malandrini A, Fabrizi GM, Brown R, Vance J, Pericak-Vance M, Rudolf G, Carre S, Alonso E, Manfredi M, Nemeth AH, Monaco AP. A conserved sorting-associated protein is mutant in chorea-acanthocytosis. Nat Genet. 2001; 28:119–120. [PubMed: 11381253]

Rieder SE, Emr SD. A novel RING finger protein complex essential for a late step in protein transport to the yeast vacuole. Molecular biology of the cell. 1997; 8:2307–2327. [PubMed: 9362071]

Roczniak-Ferguson A, Petit CS, Froehlich F, Qian S, Ky J, Angarola B, Walther TC, Ferguson SM. The transcription factor TFEB links mTORC1 signaling to transcriptional control of lysosome homeostasis. Sci Signal. 2012; 5:ra42. [PubMed: 22692423]

Rutherford NJ, Carrasquillo MM, Li M, Bisceglio G, Menke J, Josephs KA, Parisi JE, Petersen RC, Graff-Radford NR, Younkin SG, Dickson DW, Rademakers R. TMEM106B risk variant is implicated in the pathologic presentation of Alzheimer disease. Neurology. 2012; 79:717–718. [PubMed: 22855871]

Sardiello M, Palmieri M, di Ronza A, Medina DL, Valenza M, Gennarino VA, Di Malta C, Donaudy F, Embrione V, Polishchuk RS, Banfi S, Parenti G, Cattaneo E, Ballabio A. A gene network regulating lysosomal biogenesis and function. Science. 2009; 325:473–477. [PubMed: 19556463]

Sato TK, Rehling P, Peterson MR, Emr SD. Class C Vps protein complex regulates vacuolar SNARE pairing and is required for vesicle docking/fusion. Molecular cell. 2000; 6:661–671. [PubMed: 11030345]

Schwenk BM, Lang CM, Hogl S, Tahirovic S, Orozco D, Rentzsch K, Lichtenthaler SF, Hoogenraad CC, Capell A, Haass C, Edbauer D. The FTLD risk factor TMEM106B and MAP6 control dendritic trafficking of lysosomes. EMBO J. 2014

Settembre C, Di Malta C, Polito VA, Garcia Arencibia M, Vetrini F, Erdin S, Erdin SU, Huynh T, Medina D, Colella P, Sardiello M, Rubinsztein DC, Ballabio A. TFEB links autophagy to lysosomal biogenesis. Science. 2011; 332:1429–1433. [PubMed: 21617040]

Settembre C, Zoncu R, Medina DL, Vetrini F, Erdin S, Erdin S, Huynh T, Ferron M, Karsenty G, Vellard MC, Facchinetti V, Sabatini DM, Ballabio A. A lysosome-to-nucleus signalling mechanism senses and regulates the lysosome via mTOR and TFEB. EMBO J. 2012; 31:1095–1108. [PubMed: 22343943]

Settembre C, De Cegli R, Mansueto G, Saha PK, Vetrini F, Visvikis O, Huynh T, Carissimo A, Palmer D, Klisch TJ, Wollenberg AC, Di Bernardo D, Chan L, Irazoqui JE, Ballabio A. TFEB controls cellular lipid metabolism through a starvation-induced autoregulatory loop. Nature cell biology. 2013; 15:647–658.

Sherer NM, Lehmann MJ, Jimenez-Soto LF, Ingmundson A, Horner SM, Cicchetti G, Allen PG, Pypaert M, Cunningham JM, Mothes W. Visualization of retroviral replication in living cells reveals budding into multivesicular bodies. Traffic. 2003; 4:785–801. [PubMed: 14617360]

Smith KR, Damiano J, Franceschetti S, Carpenter S, Canafoglia L, Morbin M, Rossi G, Pareyson D, Mole SE, Staropoli JF, Sims KB, Lewis J, Lin WL, Dickson DW, Dahl HH, Bahlo M, Berkovic SF. Strikingly different clinicopathological phenotypes determined by progranulin-mutation dosage. Am J Hum Genet. 2012; 90:1102–1107. [PubMed: 22608501]

Thoreen CC, Kang SA, Chang JW, Liu Q, Zhang J, Gao Y, Reichling LJ, Sim T, Sabatini DM, Gray NS. An ATP-competitive mammalian target of rapamycin inhibitor reveals rapamycin-resistant functions of mTORC1. J Biol Chem. 2009; 284:8023–8032. [PubMed: 19150980]

Um JW, Nygaard HB, Heiss JK, Kostylev MA, Stagi M, Vortmeyer A, Wisniewski T, Gunther EC, Strittmatter SM. Alzheimer amyloid-beta oligomer bound to postsynaptic prion protein activates Fyn to impair neurons. Nat Neurosci. 2012; 15:1227–1235. [PubMed: 22820466]

Um JW, Kaufman AC, Kostylev M, Heiss JK, Stagi M, Takahashi H, Kerrisk ME, Vortmeyer A, Wisniewski T, Koleske AJ, Gunther EC, Nygaard HB, Strittmatter SM. Metabotropic glutamate receptor 5 is a coreceptor for Alzheimer abeta oligomer bound to cellular prion protein. Neuron. 2013; 79:887–902. [PubMed: 24012003]

Urwin H, Authier A, Nielsen JE, Metcalf D, Powell C, Froud K, Malcolm DS, Holm I, Johannsen P, Brown J, Fisher EM, van der Zee J, Bruyland M, Consortium FR, Van Broeckhoven C, Collinge J, Brandner S, Futter C, Isaacs AM. Disruption of endocytic trafficking in frontotemporal dementia with CHMP2B mutations. Hum Mol Genet. 2010; 19:2228–2238. [PubMed: 20223751]

Van Deerlin VM, et al. Common variants at 7p21 are associated with frontotemporal lobar degeneration with TDP-43 inclusions. Nat Genet. 2010; 42:234–239. [PubMed: 20154673]

van der Zee J, Van Langenhove T, Kleinberger G, Sleegers K, Engelborghs S, Vandenberghe R, Santens P, Van den Broeck M, Joris G, Brys J, Mattheijssens M, Peeters K, Cras P, De Deyn PP, Cruts M, Van Broeckhoven C. TMEM106B is associated with frontotemporal lobar degeneration in a clinically diagnosed patient cohort. Brain. 2011; 134:808–815. [PubMed: 21354975]

Vass R, Ashbridge E, Geser F, Hu WT, Grossman M, Clay-Falcone D, Elman L, McCluskey L, Lee VM, Van Deerlin VM, Trojanowski JQ, Chen-Plotkin AS. Risk genotypes at TMEM106B are associated with cognitive impairment in amyotrophic lateral sclerosis. Acta Neuropathol. 2011; 121:373–380. [PubMed: 21104415]

Wang IF, Guo BS, Liu YC, Wu CC, Yang CH, Tsai KJ, Shen CK. Autophagy activators rescue and alleviate pathogenesis of a mouse model with proteinopathies of the TAR DNA-binding protein 43. Proc Natl Acad Sci U S A. 2012; 109:15024–15029. [PubMed: 22932872]

Westphal V, Rizzoli SO, Lauterbach MA, Kamin D, Jahn R, Hell SW. Video-rate far-field optical nanoscopy dissects synaptic vesicle movement. Science. 2008; 320:246–249. [PubMed: 18292304]

Yamada K, Matsushima R, Nishimura M, Hara-Nishimura I. A slow maturation of a cysteine protease with a granulin domain in the vacuoles of senescing Arabidopsis leaves. Plant Physiol. 2001; 127:1626–1634. [PubMed: 11743107]

Zdolsek JM, Olsson GM, Brunk UT. Photooxidative damage to lysosomes of cultured macrophages by acridine orange. Photochemistry and photobiology. 1990; 51:67–76. [PubMed: 2304980]

Highlights

- TMEM106B regulates neuronal lysosome size, number and transport
- Increased TMEM106B causes TFEB nuclear translocation to enhance lysosomal gene expression
- Loss of TMEM106B delays Torin-induced TFEB nuclear translocation
- Neuronal TMEM106B protects lysosomes from oxidative photodamage

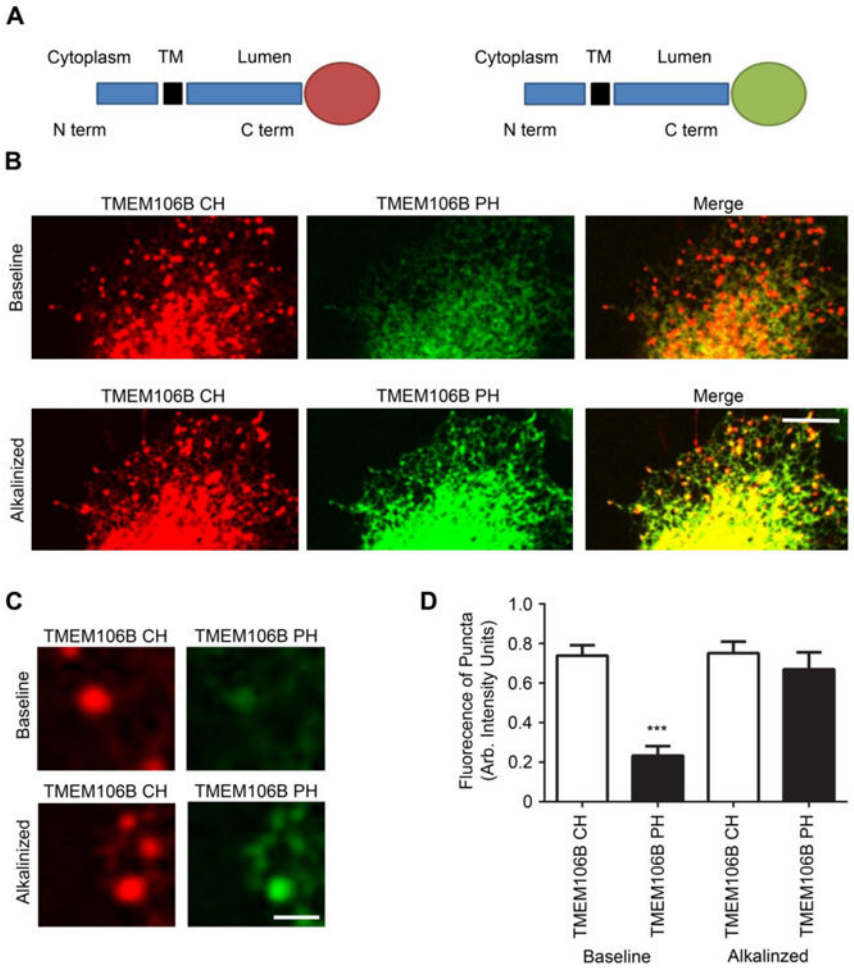

Figure 1. Topology of TMEM106B

(A) Schematic of fluorescent fusion protein constructs of TMEM106B with Cherry (red) or pHluorin (green) tag and deduced membrane orientation. TM, transmembrane.

(B, C) COS-7 cells were transfected with expression vectors for TMEM106B-Cherry (red) and TMEM106B-pHluorin (green) and then imaged in time lapse without fixation 48 hours later. Prior to addition of 500 nM bafilomycin A1 and 0.075% (w/v) sodium bicarbonate, the red fluorescence is intense and the green signal is quenched. Twenty minutes after alkalinization of the lysosomal lumen, green fluorescence is increased. Panel C shows a higher magnification of individual puncta from B. Scale bars, 15 μm in B and 2 μm in C.

(D) The fluorescence intensity in the Cherry and pHluorin channels from experiments as in B, C was measured for regions generated from a threshold mask in the red channel. Data are mean ± sem from n = 7 independent experiments. One-way ANOVA with post-hoc pairwise testing relative to vector control, **, $P \leq 0.01$.

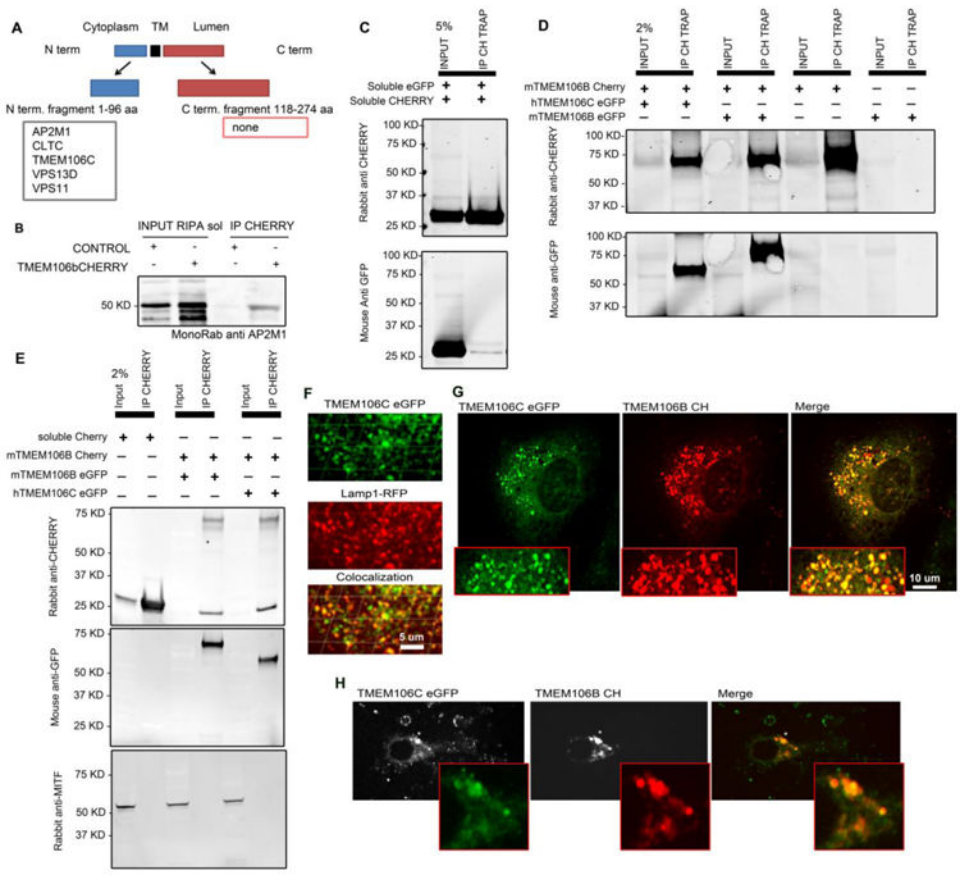

Figure 2. TMEM106 Forms Mulitmers and Interacts with Endocytic Adaptors

(A) Schematic of Y2H screening results using the C terminal and N terminal fragments of TMEM106B against a human clone library derived from multiple tissues including brain. Positive interactions ranked with a confidence score between the two fragment are listed in figure.

(B) Extracts of HEK293 cells transfected with empty vector or TMEM106B-Cherry expression vector were analyzed by anti-RFP/CHERRY immunoprecipitation (IP) and immunoblot with anti-AP2M1 antibodies. 5% input analyzed.

(C) Extracts of HEK293 cells transfected with soluble eGFP and soluble Cherry expression vector were analyzed by anti-RFP/CHERRY immunoprecipitation (IP) and immunoblot with anti-Cherry and anti-GFP antibodies. 5% input analyzed.

(D, E) Extracts of HEK293 cells transfected with the indicated tagged TMEM106B and TMEM106C expression vectors were analyzed by anti-RFP/CHERRY immunoprecipitation (IP) and immunoblot with anti-Cherry and anti-GFP antibodies, or with anti-MITF antibody. 2% input analyzed.

(F) COS-7 cells co-expressing TMEM106B-eGFP (green) and LAMP1-RFP (red) were imaged by confocal microscopy and a three dimensional image reconstructed form a z-series The peripheral zone of the cell is illustrated at high magnification. Scale bar is 5 μm.

(G) COS-7 cells co-expressing TMEM106B-Cherry (red) and TMEM106C-eGFP (green) were imaged by confocal microscopy. The entire cell shown in the larger panel and higher magnification is provided in the insets. Scale bar is 10 μm for main panel and 5 μm for inset.

(H) Cortical neurons were transfected with expression vectors for TMEM106B-Cherry (red) and TMEM106C-eGFP (green) and imaged at DIV20 by confocal microscopy. The entire cell soma shown in the larger panel and higher magnification is provided in the insets.

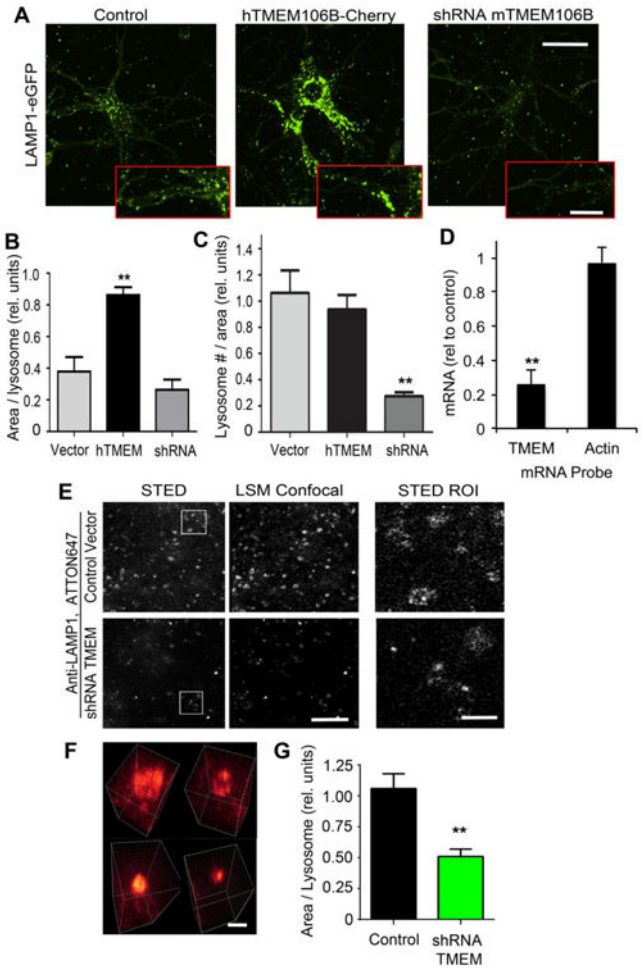

Figure 3. TMEM106B Levels Determine Lysosome Size and Number in Neurons

(A) Mouse E18 cortical neurons were transfected with expression vectors for empty U6-shRNA control vector, TMEM106B-Cherry vector or U6-shRNA TMEM106B targeting vector, together with LAMP1-eGFP (green) and then imaged in time lapse without fixation 20 days later. A higher magnification view is proved in the inset. Scale bars, 15 μm for main panel and 5 μm for inset.

(B, C) Measurement of the area per lysosome, and number of lysosomes per cellular area was determined from experiments as in A. Data are relative units for mean ± sem from n = 6-8 independent experiments. One-way ANOVA with Tukey post-hoc pairwise testing relative to vector control, **, $P \leq 0.01$.

(D) Mouse E18 cortical neurons were transfected with expression vectors for empty U6-shRNAcontrol vector, or U6-shRNA TMEM106B targeting vector, and then mRNA levels were after 20 days by RT-PCR. The level for TMEM106B and actin is plotted as a ratio between TMEM106B targeting vector and control vector. Data are mean ±sem from n = 3 independent experiments.

Student's two tailed *t* test, **, $P \leq 0.01$.

(E) Mouse E18 cortical neurons were transfected A with control vector or shRNA vector for TMEM106B, and after 20DIV stained for anti-LAMP1 using an ATTON647-tagged

secondary antibody. Images were collected by STED microscopy and by standard laser scanning microscopy in the left and middle panels. Higher magnification of the boxed regions from the STED image are shown at right. Scale bar, 5 μm for main panels and 1.5 μm for boxed ROI.

(F) Representative 3D view of different lysosome structure captured by STED.

(G) Measurement of average lysosomal area measured by STED. Data are mean ± sem from n = 4-6 independent experiments. Student's two tailed *t* test, **, $P \leq 0.01$.

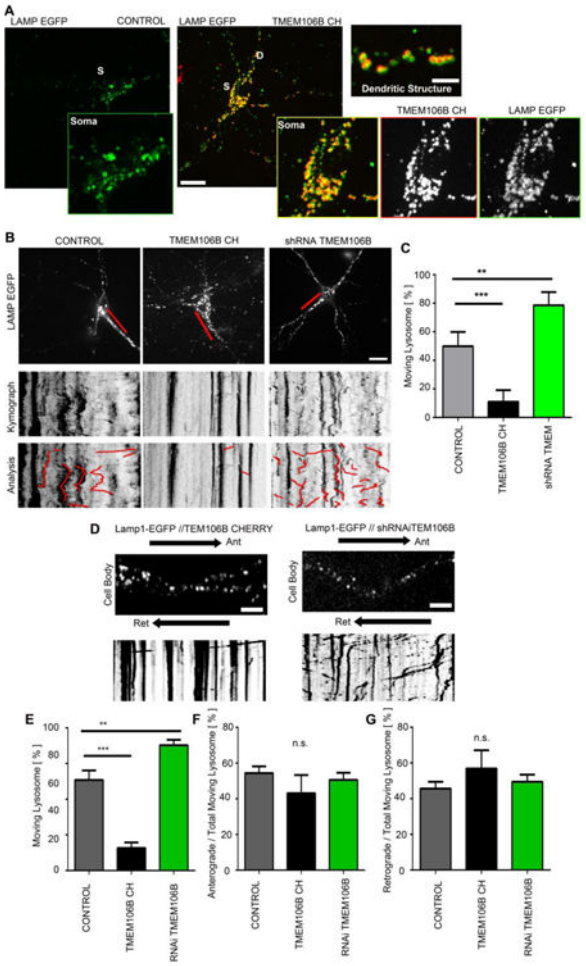

Figure 4. TMEM106b Expression Titrates Lysosome Transport in Neurites

(A) Mouse E18 cortical neurons were transfected with an expression vector encoding LAMP1-eGFP together with empty control vector, TMEM106B-Cherry vector or U6-shRNA TMEM106B targeting vector. At 20DIV, images of live neurons from Control and TMEM106B-Cherry were obtained by spinning disc confocal microscopy. The cell soma (S) and the dendrites (D) show puncta scored as lysosomes, seen at higher magnification in the insets. Note that in the TMEM106B overexpressing situation, LAMP1-eGFP strucutres are larger and colocalize with TMEM106B-Cherry. Scale bar, 10 μm for main panels and 5 μm for the soma insets and 2 μm for the dendrite inset.

(B) Neurons as in A were imaged in time lapse at 20DIV. The red bars in the top panels indicate the proximal 20 μm segment utilized to generate the kymograph in the bottom panels. Images were captured at a rate of one per 3 sec for 450 sec. Scale bar, 10 μm. The kymographs (inverted image) reflect LAMP1-positive organelle movement with over 20 μm in the *x*-axis, and 450 sec in the *y*-axis. See Movie 4. The analysis of lysosomal movement is illustrated by the red overlay on the image in the bottom panels.

(C) The percentage of lysosomes with transport movements detected in 20 μm by 450 seckymographs as in A is depicted. Data are mean ± sem from n = 6 independent

experiments. Oneway ANOVA with Tukey post-hoc pairwise testing relative to vector control, $^{**}P \leq 0.01$, $^{***}P \leq 0.001$.

(D) Mouse cortical neurons were cultured transfected and imaged as in A and B, but cultures were low density and imaging was at DIV8. The LAMP1-eGFP channel is shown for a segment of dendrite adjacent to the cell some to the left of the image. Anterograde and retrograde directions areindicated. The lower panels are kymographs of LAMP1 movement over 20 μm in the *x*-axis, and 450sec in the *y*-axis.

(E-G) The percentage of lysosomes with transport movements detected over a 450 sec kymographs as in D. Data are mean ± sem from n = 10. One-way ANOVA with Tukey post-hoc pairwise testing relative to vector control, $^{**}P \leq 0.01$, $^{***}P \leq 0.001$. The fraction of anterograde (F) and retrograde (G) movements relative to total lysosome movements is plotted from the same analysis.

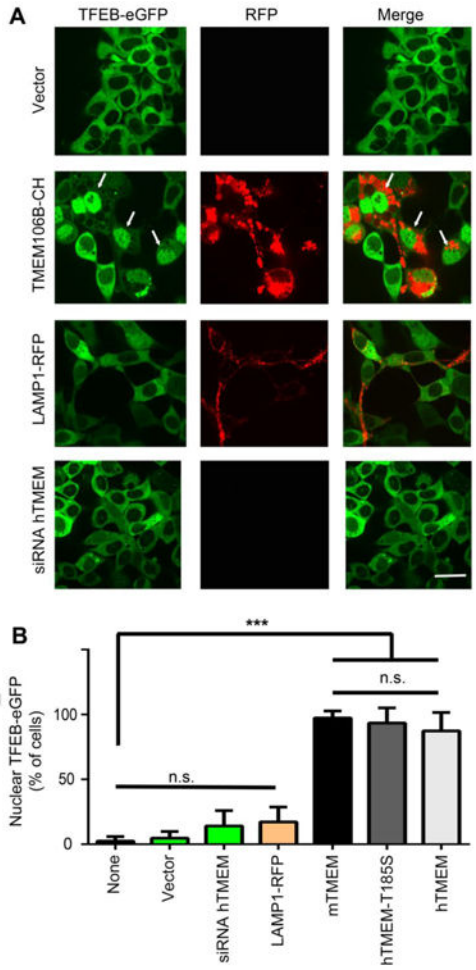

Figure 5. TMEM106B induces TFEB translocation in 293 cell lines

(A) HEK293 cells stably expressing TFEB-eGFP were transiently transfected with expression vectors for mouse TMEM106B-Cherry or LAMP1-RFP or empty vector or with siRNA pools targeting human TMEM106B. After 24-36 hours, confocal images were acquired. Note that in control vector cells, TFEB-eGFP is cytoplasmic while in TMEM106B-Cherry overexpressing cells the protein is detected in the nucleus (arrows). Scale bar, 10 μm.

(B) The percentage of cells with nuclear TFEB-eGFP signal from experiments as in A is plotted as a function of transient transfection condition. In addition to the conditions from A, additional co-expressed vectors encoded human TMEM106B and human TMEM106B-T185S variant. Data are mean ± sem from n = 8-24 independent experiments. One-way ANOVA with Tukey post-hoc pairwise testing as indicated, ***$P \leq 0.001$.

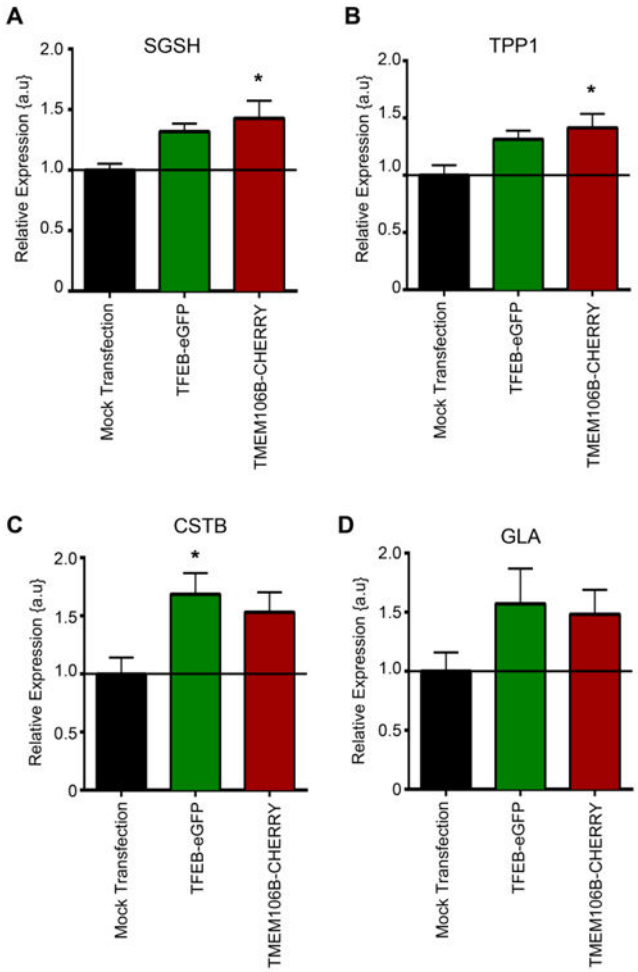

Figure 6. TMEM106b overexpression activates CLEAR network genes in HEK293-T Cells

(A-D) HEK293 cells transiently transfected with empty expression vector for mock transfection, TMEM106b-Cherry or TFEB-eGFP. Gene expression for the four indicated genes was analyzed by quantitative PCR and normalized to ACTB and expressed as relative expression (control = 1) to determine changes in expression of select CLEAR network genes. Experiments were performed in duplicate with n=3 per transfection condition (data expressed as mean + sem). One-way ANOVA with Bonferonni post-hoc test for multiple comparisons was performed, *P<0.05.

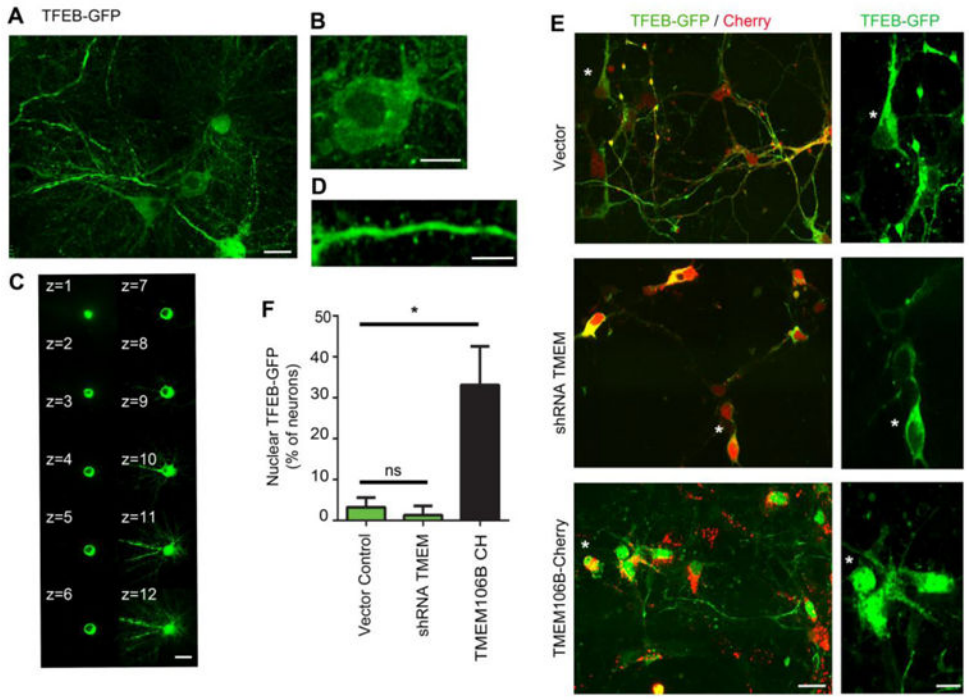

Figure 7. TMEM106B induces TFEB translocation in neurons

(A-D) Mouse E18 cortical neurons were transfected with an expression vector for TFEB-GFP and then imaged with a confocal microscope at 20DIV. The wide field view in A illustrates both cell soma and neurite fluorescence. Cell soma with negative nuclear signal is observed at higher magnification in B, and a 0.5 μm step Z-series through the cell soma in C verifies the nuclear void of fluorescence. Higher magnification view of a dendrite in D includes filling of spine-like structures. Scale bar, 10 μm in A, C and 5 μm in B, D.

(E) Mouse E18 cortical neurons were transfected with an expression vector encoding TFEB-GFPtogether with expression vectors for empty U6-shRNA control vector plus soluble Cherry expressionvector, or U6-shRNA TMEM106B targeting vector plus soluble Cherry expression vector, orTMEM106B-Cherry fusion protein. Live confocal images of the neurons were acquired at 20DIV. Lowmagnification views with both the TFEB-GFP (green) and the Cherry (red) channel are at left, andhigher magnification views of the TFEB localization is at right. The asterix indicated the neuronvisualized in both panels. Scale bar, 10 μm for the left panel and 5 μm for the right panel.

(F) The percentage of neurons with nuclear TFEB-eGFP signal from experiments as in E is plotted.Data are mean ±sem from n = 5-6 independent experiments. One-way ANOVA with Tukey post-hocpairwise testing as indicated, *$P \leq 0.05$.

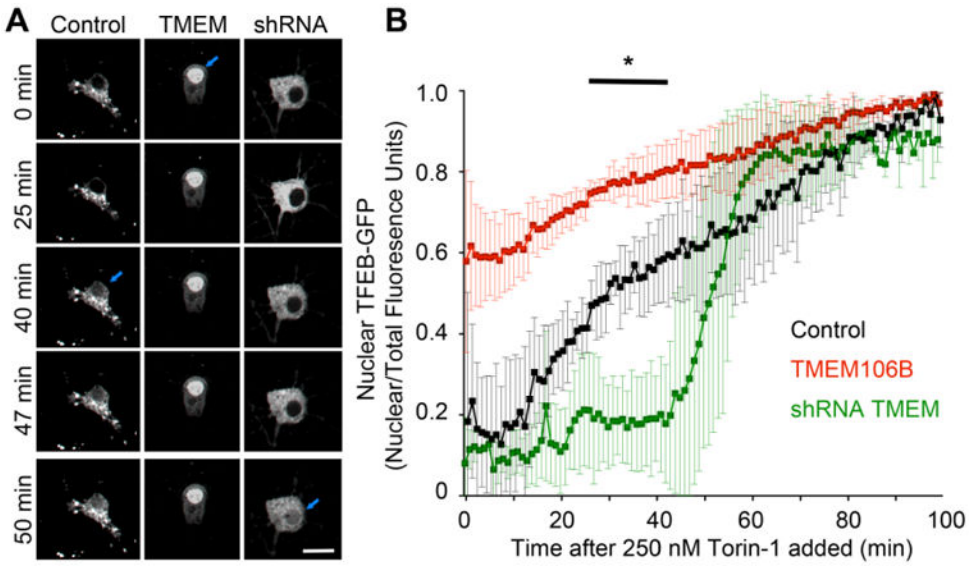

Figure 8. TMEM106B sensitizes neurons to Torin-1-induced TFEB translocation

(A) Mouse E18 cortical neurons were transfected with an expression vector encoding TFEB-GFPtogether with expression vectors for empty control vector, or TMEM106B-Cherry fusion protein (TMEM) or U6-shRNA TMEM106B (shRNA). Time-lapse images at were acquired over 120 minutes (one per min) beginning at the time of addition of 250 nM Torin-1. The soma of one neuron from eachcondition is illustrated as a function of time. The first point at which nuclear TFEB-GFP is apparent isindicated by the blue arrows. Scale bar, 10 μm.

(B) The fluorescence intensity of nuclear TFEB-eGFP signal as a ratio to total cell soma GFP signal isplotted as a function of time from experiments as in A. Data are mean ± sem from n = 4-6independent experiments. At the times indicated by the bar, the TMEM106B overexpression and shRNA values are significantly different from the control group. One-way ANOVA with Tukey post-hoc pairwise testing, $*P \leq 0.05$.

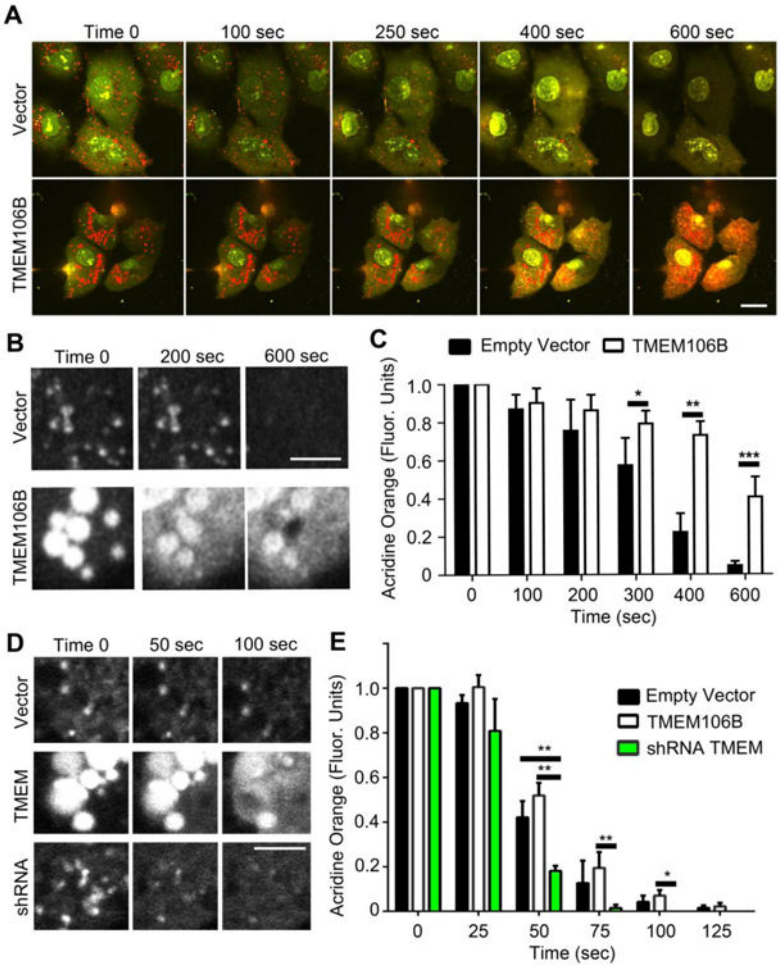

Figure 9. TMEM106B regulates lysosomal sensitivity to photo-oxidation of acridine orange

(A, B) HEK293 cells transfected with empty vector or untagged TMEM106B expression vector andafter 24-36 hours were loaded with acridine orange. Time-lapse confocal images were acquired over5 minutes (one per 5 sec) during constant illumination with 488 nm light. Acridine orange accumulation in lysosomes is detected with rhodamine filters (red) at time zero, and the lysosomes are larger with TMEM106B expression. The fluorescein filter channel (green) reflects dye in non-acidic compartments of the cell including the nucleus and cytoplasm. Lysosomal signal is rapidly lost in control cells and but is still detected at 5 minutes in TMEM106B overexpressing cells. Higher magnification views of the red channel are shown in B as gray scale. Scale bar, 2 μm. See full time series in Movie 5.

(C) The intensity of rhodamine channel fluorescence reflecting lysosomal acridine orange was measured as a function of time from experiments as in A. Data are normalized to time zeromeasurements and are mean ±sem from n = 6 independent experiments. One-way ANOVA with Tukey post-hoc pairwise testing as indicated, $*P \leq 0.05$, $**P \leq 0.01$, $***P \leq 0.001$.

(D) Mouse E18 cortical neurons were transfected with expression vectors for empty control vector, oruntagged TMEM106B fusion protein (TMEM) or U6-shRNA TMEM106B (shRNA). Neurons were loaded with acridine orange at 20DIV, and then imaged with

constant 488 illumination as in A with image acquisition in the rhodamine channel over 3 min. Higher magnification views of cell soma lysosomes in the rhodamine channel are illustrated for the indicated time points. Scale bar, 2 μm.

(E) The intensity of rhodamine channel fluorescence reflecting lysosomal acridine orange was measured as a function of time from neuronal experiments as in D. Data are normalized to time zero measurements and are mean ± sem from n = 8 independent experiments. One-way ANOVA with Tukey post-hoc pairwise testing as indicated, $*P \leq 0.05$, $**P \leq 0.01$.